Design and Development of an Earth Based Experimental Setup for Testing Algorithms on Space Robots

Francis James
International Institute Of Information Technology
Hyderabad
Telangana, India
francisjames10@gmail.com

Shubham Vyas
SRM University
Chennai
Tamil Nadu, India
shubham143@gmail.com

Puneeth Bandikatla
Birla Institute of Technology and Science
Pilani
Rajasthan, India
pbandikatla@gmail.com

P Mithun
International Institute Of Information Technology
Hyderabad
Telangana, India
mithun.p@research.iiit.ac.in

S V Shah
International Institute Of Information Technology
Hyderabad
Telangana, India
surilshah@iiit.ac.in

ABSTRACT

In space robots, coupling between the base and the arms causes the floating base to translate and rotate when the arms execute a maneuver, which is typically not seen in earth based robots. Since it is difficult to test developments in space robotics primarily due to the high cost and lack of access to robots in space, it is necessary to have physical systems that can mimic space conditions for experimental validation on earth. Among several options, the use of air bearings to build floating-base robots is one of the most effective. We describe the development of one such system that replicates zero gravity conditions for planar robots. Although similar systems exist elsewhere, the planar dual-arm space robot we have built is distinctive by being relatively lightweight, compact and modular. The setup can be used to test a wide range of experiments such as visual servoing, reactionless maneuvering and object grasping in space. In this paper, the approach taken during the development of both the hardware and software for the experimental setup are discussed. A few results obtained by numerical simulations as well as experimentation are also presented.

Keywords

Space robots, dual arm, air bearings, floating base

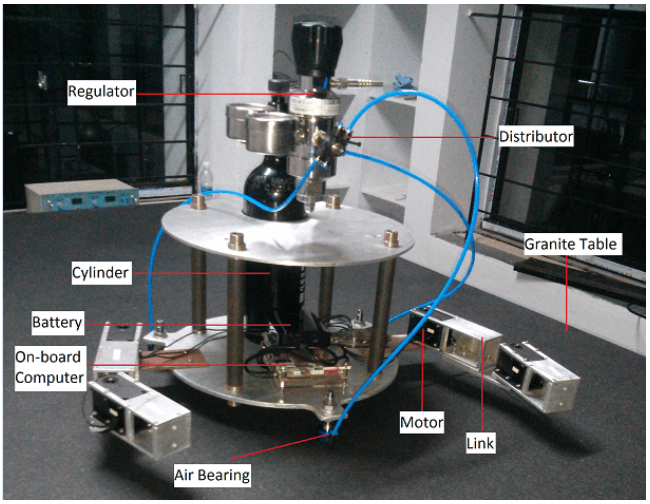

Figure 1: Earth Based Prototype of a Planar Dual-Arm Space Robot

1. INTRODUCTION

Robots in space can be used to perform several operations such as debris removal, refueling, inspection and other on-orbit services [1] [2] [3]. On space robots, which have a floating base, the motion of the arms induces rotation and translation of the base in accordance with the law of conservation of angular momentum. It is necessary to have methods and algorithms that take this coupling into consideration, especially for robots such as Dextre [4] and ETS-VII [5] [6] where it is significant. Several studies on reactionless manipulation [6], dynamic singularity avoidance [7] and visual servoing [8] have been performed for space robots in the past. Most of these studies are carried out by performing numerical simulations as it is expensive and risky to test developments directly on robots in space. Since it is not always possible to test these simulations on real space robots as in [9], we need specialized systems that can mimic microgravity conditions on earth.

A microgravity environment can be recreated using neutral buoyancy tanks, parabolic flights, gravity compensation mechanisms, magnetic levitation or the use of air bearings. Neutral buoyancy tanks allow motion in 3-D space to be

AIR '15, July 02 - 04, 2015, Goa, India

DOI: http://dx.doi.org/10.1145/2783449.2783487

tested easily, but the viscous forces hamper motion, giving an unrealistic picture of the motion of a space robot. Parabolic flights are expensive, of short durations, and infeasible for repeated testing. Gravity compensation mechanisms suffer from mechanism singularities and imperfections. While planar simulators such as magnetic levitation and air bearings can mimic microgravity conditions more accurately than these spatial systems, they only allow rotation about one axis and translation about two. Magnetic suspension systems offer a smaller range of motion than air bearings [10], making air bearings the best choice among the two. Systems using air bearings that allow three dimensional tests have also been proposed [11] [12], but they have not been successfully constructed yet.

Air bearings have been used for testing of various functions of satellites such as attitude dynamics and control at Georgia Institute of Technology [13] [14][15] and NTUA Greece [7]. Studies on guidance and navigation control have also been done at Rensselaer Polytechnic Institute [16]. The Polish Academy of Sciences developed a planar test bed with a robotic manipulator with two long links [17].

This paper presents the design and development of one such robot which uses planar air bearings to float on a smooth granite table, allowing us to study attitude changes while maneuvering. In the long run, we plan to use this setup to verify our numerical simulations on reactionless maneuvering and visual servoing with minimal attitude disturbance. The presented design is simple, lightweight and modular, allowing easy addition or removal of links and on-board electronic or mechanical components. The links also have provisions for adding grapplers and 'eye-in-hand' cameras required for visual servoing. The basic assembly is shown in Fig. 1. To the best of the authors' knowledge, this is the first testbed of its kind in India. The total mass of the entire system with two arms consisting of three links each is about 8 kg. The base including the electronics and a filled cylinder weigh a little over 5 kg, making this one of the most lightweight setups. In comparison, the robot used at NTUA weighs about 14 kg [7] and the robot at the Polish Academy of Sciences weighs 18.9 kg [17], although the link lengths are considerably larger for the latter. Our system maintains a mass distribution ratio, defined as the ratio of the combined mass of the arms to the mass of the base, of about 0.4 which is comparable to the one in [17] and is large enough to cause significant coupling. These and some other parameters are listed in Table 1.

The paper is divided into six sections. First, the mathematical preliminaries of a space robot are presented. Next, the hardware design of the robot is explained, followed by the on-board electronics. Further, the current development of the robot is presented along with the initial experimentation. Finally, the results obtained are presented along with the scope of future work.

2. MATHEMATICAL PRELIMINARIES

For an n-Degrees-Of-Freedom (n-DOF) robotic system mounted on a floating-base, linear and angular momenta ($\boldsymbol{p}$ and $\boldsymbol{l}$ respectively) are given by [6]

$$\begin{bmatrix} \boldsymbol{p} \\ \boldsymbol{l} \end{bmatrix} = \boldsymbol{I}_b \boldsymbol{t}_b + \boldsymbol{I}_{bm} \dot{\boldsymbol{\theta}} + \begin{bmatrix} \boldsymbol{0} \\ \boldsymbol{r_0} \times \boldsymbol{p} \end{bmatrix} \tag{1}$$

where $\boldsymbol{I}_b \in R^{6\times 6}$ is the inertia matrix of the floating-base, $\boldsymbol{I}_{bm} \in R^{6\times n}$ is the coupling inertia matrix, $\boldsymbol{t}_b \in R^6$ is the twist vector containing linear velocity ($\boldsymbol{v}_0$) and angular velocity ($\boldsymbol{\omega}_0$) of the base, and $\dot{\boldsymbol{\theta}} \in R^n$ is the vector of joint velocities.

In the absence of external forces, the linear and angular momenta remain constant. (1) clearly shows that joint motion can induce base motion in accordance with momentum conservation laws. The end-effector motion can be mapped to the joint motion while accounting for translations and rotations of the base using the Generalised Jacobian Matrix (GJM), given by [18]

$$\boldsymbol{t}_e = \boldsymbol{J}_g \dot{\boldsymbol{\theta}}, \ \textit{where } \boldsymbol{J}_g = \left(\boldsymbol{J}_{me} - \boldsymbol{J}_{be}\boldsymbol{I}_b^{-1}\boldsymbol{I}_{bm}\right). \tag{2}$$

In (2), $\boldsymbol{t}_e$ is the twist vector containing linear and angular velocities of the end effector, $\boldsymbol{J}_g$ is the GJM, and $\boldsymbol{J}_{be}$ and $\boldsymbol{J}_{me}$ are the Jacobian matrices for the base and manipulator, respectively. The base velocity is given by [18]

$$\boldsymbol{t}_b = \boldsymbol{J}_{be}^{-1}(\boldsymbol{t}_e - \boldsymbol{J}_{me}\dot{\boldsymbol{\theta}}) \tag{3}$$

where $\boldsymbol{t}_b$ is the base twist vector.

Simulations were performed using (1) to (3) on a space robot. The physical parameters such as inertias were obtained from the CAD model. Although the the simulations were performed in joint space, (2) can be used to design trajectories in Cartesian space.

3. MECHANICAL DESIGN

Space robots like Dextre and ETS VII typically house most of the electronics and sensors on the base of the robot, which accounts for most of the mass. The remaining mass is distributed among the arms. Although this mass is lower, it is still significant enough to cause base reactions. Our robot has a similar mass distribution. Some of the parameters of various parts of the robot are given in Table 1.

Parameter	Value
Total Mass (with 75% filled cylinder)	8.050 kg
Link Length (end link)	10.00 cm
Link Length (others)	15.00 cm
Link Mass (end link)	0.195 kg
Link Mass (others)	0.305 kg
Mass of Motor	0.126 kg
Mass ratio (mass of arms/mass of base)	0.415

Table 1: Geometric and Mass Parameters

The base of the robot is made of aluminum and has a cylindrical shape formed by circular discs mounted on the base using four steel rods. Both the base and the arms of the space robot were designed keeping in mind the scope for future expansion. Discs can be stacked vertically or removed depending on the amount of usable volume required for the experiment. Similarly, a modular design allows us to add more links to each arm if desired. Spring steel connectors are used to attach the arms to the base to allow flexural bending, ensuring planarity of the arms and the base when air bearings are attached to the arms. The robot base is supported by three air bearings mounted below the base. Each

arm has an air bearing support at the center link. More links can be attached to each arm. The CAD model shown in Fig.2 has two arms consisting of three links each.

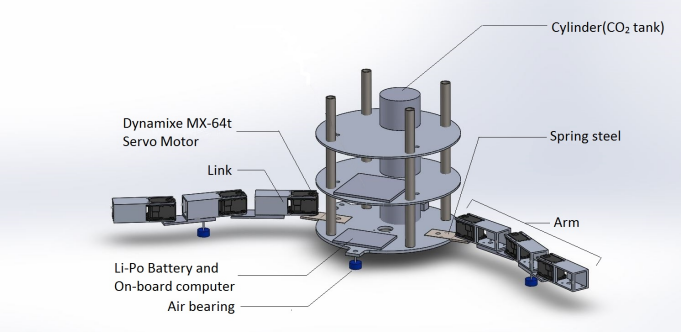

Figure 2: CAD Model of the Robot

3.1 Air Bearing

Air bearings use a thin film of pressurized air to provide an exceedingly low friction load-bearing interface between surfaces. This ensures that the robot and the granite floor do not touch. For this design, porous air bearings were used as they exhibit many advantages over orifice air bearings such as uniform pressure distribution over the entire surface, higher immunity to scratches and less chance of clogging . Air bearings of 25mm diameter were selected due to their small size and high load bearing capacity. Each of these bearings is capable of liftng loads up to 80N to a height of 5 microns when supplied with air or any gas such as carbon dioxide at a pressure of 0.41 MPa (60 psi). The air bearing is placed in an Aluminum housing and uses porous carbon to distribute the flow. Three air bearings, placed using ball and stud mounting in triangular fashion below the base of the robot, are used to support the base of the robot. In addition to this, one air bearing can be used to support each link individually.

3.2 Granite Table

As the air bearings produce a film of thickness 5 microns, the robot would require an extremely flat surface to float upon. This flatness would have to be microscopic, since the local roughness of the surface should be less than 16 RMS and macroscopic, in order to avoid wavy surfaces which would render the robot unstable. Possible solutions were using epoxy test bed or granite slab. Granite slab was chosen due to unavailability of professionals making epoxy testbeds locally. A granite slab of dimensions 1.8m x 1m x 0.2m with a flatness of 5.69 microns was acquired and can be seen in Fig. 1. The supporting frame of the granite slab is fitted with leveling screws so as to allow the granite slab to be adjusted, thus ensuring that the gravitational forces do not cause any drifting.

3.3 Robot Base

The base of the robot consists of circular discs made of aluminum stacked using cylindrical rods made of mild steel. This provides modularity and large volume for placing the pneumatic components such as carbon dioxide cylinder, regulator, distributor as well as electronic components such as

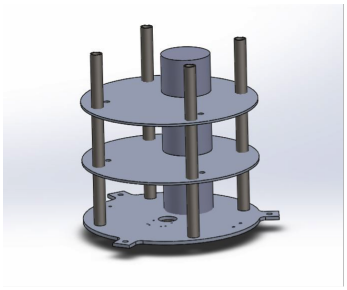

Figure 3: Robot Base

onboard computer, optical sensors and battery. When plates are stacked to form a 3-floor structure as shown in Fig.3, the base has 22 liters of available volume for the components. The compressed carbon dioxide cylinder is off-centered to provide more room for electronic systems. The weight of the cylinder is balanced by placing the regulator and battery on the opposite end so as to make sure the center of mass is as close to the geometric center as possible. The mass distribution of the base is such that the center of mass does not go beyond the air bearing supports in any configuration for arms comprising of up to three links of the specified dimensions, thus making the robot stable during maneuvers even if no air bearings are provided on the arms.

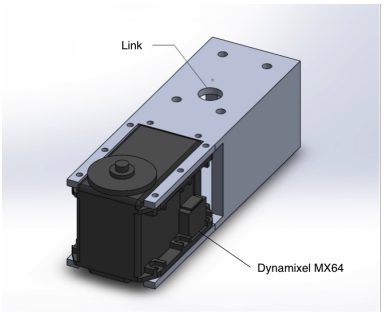

Figure 4: CAD Model of the Link

3.4 Link Design

Each link accommodates one Dynamixel MX64T actuator, and has provision for an air bearing shaft. Hollow structure has been used to allow easy access to the motors and shafts and also to ensure that the arms do not weigh more than the base. All links except the last link are 15 cm in length. The last link is 10 cm long and has provisions for attaching cameras and an end-effector such as a gripper. Fig. 4 shows one of the intermediate arms with the bottom side facing up and Table 2 lists its inertia parameters.

Inertia Parameters ($g\ mm^2$)		
$I_{xx} = 95250.05$	$I_{xy} = 102.17$	$I_{xz} = 3751.08$
$I_{yx} = 102.17$	$I_{yy} = 90478.56$	$I_{yz} = 114.92$
$I_{zx} = -3751.08$	$I_{zy} = 114.92$	$I_{zz} = 41624.08$

Table 2: Inertia Parameters of an Intermediate Link

3.5 Reaction Wheel

A reaction wheel can be used to control the rotation of base during experimentation by using the principle of conservation of angular momentum. It is placed below the bottommost base plate. The size of the reaction wheel had to be kept as small as possible to avoid collision with optical sensors and air bearings. When it detects the rotation of base, it rotates in the opposite direction to counteract the base rotation. Note that the reaction wheel was detached while performing the experiments presented in this paper. The position of the reaction wheel is shown in Fig. 5.

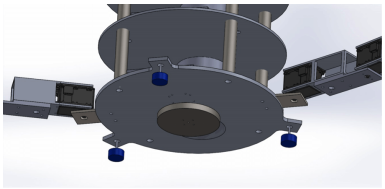

Figure 5: Reaction Wheel

3.6 Pneumatic System

Carbon dioxide is fed to the air bearings to make the robot float over the granite surface. A small cylinder containing liquid carbon dioxide is placed on the base of the robot and supplies carbon dioxide at saturation pressure to the regulator which reduces the pressure to 0.41 MPa and then supplies it to the distributer. Tubes of equal length connect the distributor outlets to the three air bearings supporting the base. Additional tubes attach to rotary pneumatic fittings before supplying carbon dioxide to the air bearings on the links to ensure unhindered rotation of the arms.

4. ELECTRICAL AND ELECTRONIC DESIGN

The space robot setup has an on-board battery powered computer which controls all the actuators. It can be used for autonomous control or for executing instructions received wirelessly from another computer. The on-board computer consists of a dual core ARM Cortex-A7 CPU with 2GB DDR3 RAM and runs a modified version of Ubuntu. It also supports a hard disk drive for data logging. It was selected due to its higher processing power compared to other boards such as Raspberry Pi or Beaglebone along with a lower power consumption due the use of RISC architecture used in the ARM processor. All the other electronic components are powered by a separate Lithium-polymer battery. The on-board computer monitors the functions of the space robot and communicates with other electronic components using serial communications protocol. It controls the actuators over USB by employing USB to serial converter. It is also used for computer vision and image processing. A high level library written in Python provides the APIs which help in control of the actuators. An overview of the power and data flow is shown in Fig. 6.

4.1 Actuator

Dynamixel MX64T motors are used for actuation of the arms. One motor is attached to each link. These motors are

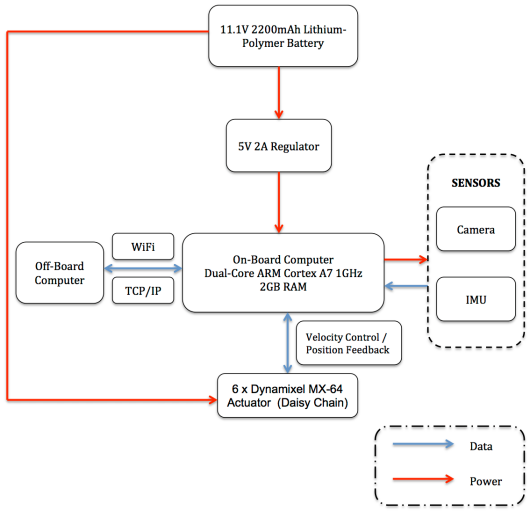

Figure 6: Power and Data Flow Diagram

Parameter	Description
Motor	Maxxon
Position Sensor	12Bit Contactless Absolute Encoder
Controller	ST CORTEX-M3
Baud Rate	1Mbps
Resolution	0.088^o
Weight	126g
Stall Torque	5.5N.m
No Load Speed	50rpm
Voltage	11.1V
Feedback	Position, Load

Table 3: Actuator Specifications

connected in a daisy chain and communicate using serial protocol. The motors are connected to the on-board computer using Serial to USB converter. They are controlled using dynamixel library written in Python. Velocity commands are sent to the motors while receiving position feedback, with the whole process occurring at 50Hz. Initial testing of trajectory following using the actuators gave position errors of less than half a degree. More details of the actuator are provided in Table 3.

4.2 Sensors

Various sensors are used to give robot a sense of its environment as well as its position in the environment. Three optical sensors, similar to ones used in optical mouse, are to be attached below the robot which detect the movement of robot in the horizontal plane using digital image correlation. Each sensor will output the distance moved and reading from two sensors can be combined to extract the translation and rotation of the space robot. The three sensors form a triangle and the translation and rotation of this triangle can be recorded. They are integrated using the GPIO pins available on the on-board computer.

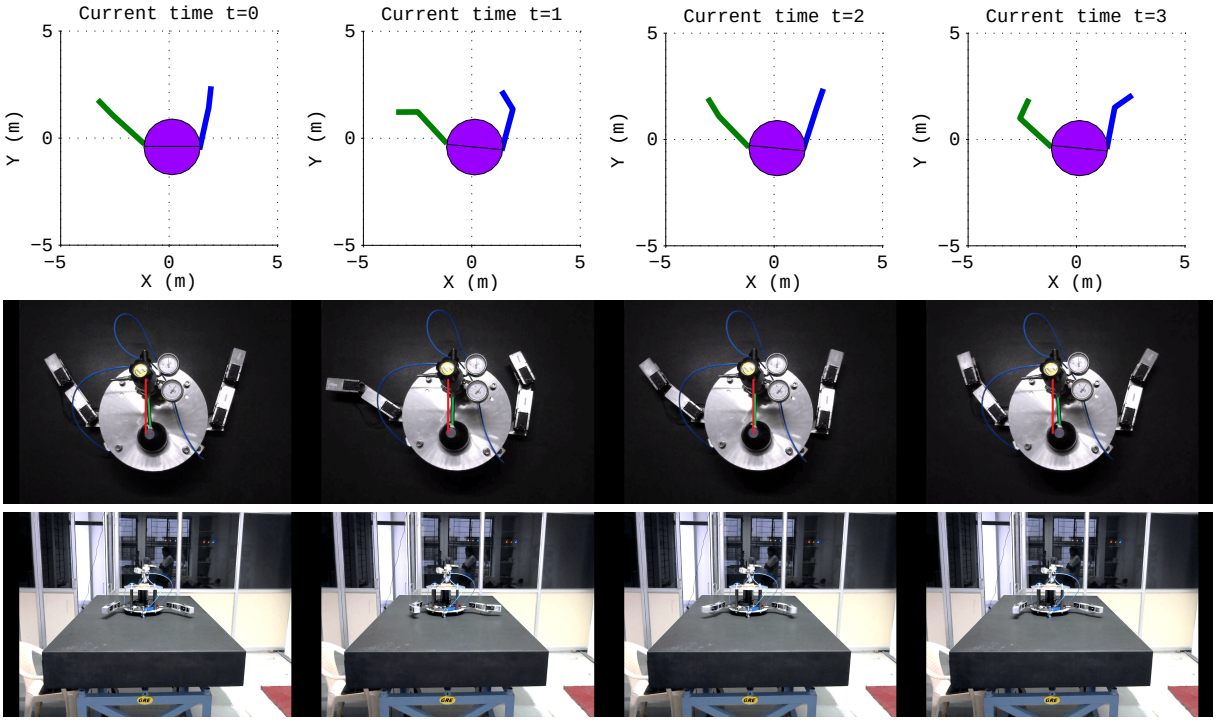

(a) 0s (b) 1s (c) 2s (d) 3s

Figure 7: Simulation results, top view and front view of the space robot at various instances of time (in seconds)

Two cameras can be mounted, each on the end of the manipulator arm. These cameras record video of resolution 640x480 at 30fps. They are connected to the on-board computer via USB and the images are processed using OpenCV. Thess 'eye-in-hand' type cameras are required for performing viual servoing operations [8].

Optional module attachment for an Inertial Measurement Unit (IMU) is provided to record changes in acceleration and angular velocity with the use of MEMS accelerometer and gyroscopes.

5. RESULTS

In order to test the setup, we ran numerical simulations for a 2-link dual arm robot and replicated the motion on the physical setup. The results obtained are presented here.

5.1 Numerical Simulation

Based on the theory presented in Section 2, numerical simulations were carried out on a dual-arm robot with two links on each arm. Sinusoidal motions with varying frequencies and amplitudes for each link were used as joint trajectories. The simulation was performed for a duration of 10 seconds and the change in state of the base and the arms obtained through the simulations are shown in Fig. 8 and Fig. 9 respectively. The first row of Fig. 7 shows snapshots of the robot at a few discrete intervals of time.

5.2 Experimentation

Experiments were carried out on a dual arm robot with two links on each arm. The optical sensors and the reaction wheel were detached for the results shown here. No cameras or grippers were added to the last link to simplify the

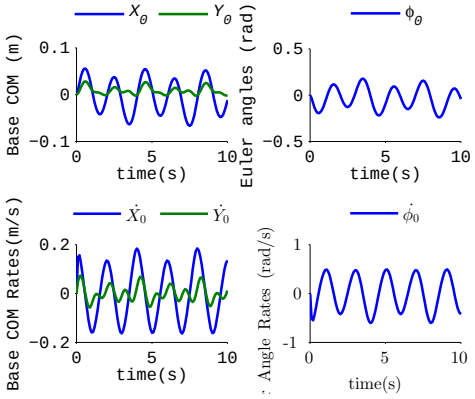

Figure 8: Rates and Positions of of the Base Centre of Mass

model. The same joint trajectories used for the simulations were replicated on the experimental setup. The sequence of images in Fig. 7 shows the translation and rotation of the base. The top view and front view of the robot at different instances of time are shown in the second and third rows of Fig. 7. The red line in the top view is fixed in space and the green line traces the pipe to the regulator. The relative position and orientation of these two lines indicate the rotation and translation of the base.

5.3 Errors

The inertia parameters of the robot calculated from the CAD model were used for the simulation. However, the CAD model did not take motor inertia into consideration.

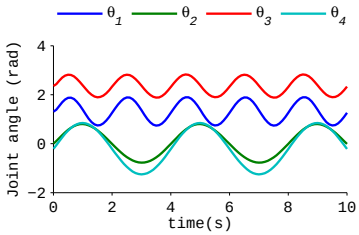

Figure 9: Joint Positions

In addition to this, it is likely that differences exist in the inertia properties obtained from the CAD model and the actual robot. These will be quantified through further experiments and measurements. The resulting errors accumulate over time and consequently, there were significant deviations after the first couple of seconds. We have presented the results till the three second mark, when these deviations become clear. More experimentation is currently being done to model the motor inertia and to gain a more accurate value of the inertia properties and will form the immediate part of our future work.

6. CONCLUSION AND FUTURE WORK

We have successfully built a testbed for a planar space robot which is lightweight and modular. The mass distribution makes the coupling between the base and the arms significant, allowing us to perform studies on attitude changes and ways to control or eliminate them. We are currently performing experiments to model the robot more accurately. Once this is done, we will begin testing the numerical results we have obtained on planar reactionless manipulation and visual servoing.

7. ACKNOWLEDGEMENTS

The authors would like to thank Nandani Kumari Roma, Research Intern at IIIT and Syed Suhail Ahmed, graduate student at VIT Vellore for their contributions at different stages of this project. This work was supported by the DST fast-track research grant No: SB/FTP/ETA-0132/2013 of the fifth author.

8. REFERENCES

[1] Shin-Ichiro Nishida, Satomi Kawamoto, Yasushi Okawa, Fuyuto Terui, and Shoji Kitamura. Space debris removal system using a small satellite. *Acta Astronautica*, 65(1):95–102, 2009.

[2] NASA Project Report. On-orbit satellite servicing study. Technical report, NASA, 2010.

[3] J-C Liou. An active debris removal parametric study for leo environment remediation. *Advances in Space Research*, 47(11):1865–1876, 2011.

[4] Elliott Coleshill, Layi Oshinowo, Richard Rembala, Bardia Bina, Daniel Rey, and Shelley Sindelar. Dextre: improving maintenance operations on the international space station. *Acta Astronautica*, 64(9):869–874, 2009.

[5] Mitsushige Oda, Kouichi Kibe, and Fumio Yamagata. Ets-vii, space robot in-orbit experiment satellite. In *Robotics and Automation, 1996. Proceedings., 1996 IEEE International Conference on*, volume 1, pages 739–744. IEEE, 1996.

[6] Kazuya Yoshida, Kenichi Hashizume, and Satoko Abiko. Zero reaction maneuver: flight validation with ets-vii space robot and extension to kinematically redundant arm. In *Robotics and Automation, 2001. Proceedings 2001 ICRA. IEEE International Conference on*, volume 1, pages 441–446. IEEE, 2001.

[7] Evangelos Papadopoulos and Steven Dubowsky. Dynamic singularities in free-floating space manipulators. In *Space Robotics: Dynamics and Control*, pages 77–100. Springer, 1993.

[8] AH Hafez, VV Anurag, SV Shah, K Madhava Krishna, and CV Jawahar. Reactionless visual servoing of a dual-arm space robot. In *Robotics and Automation (ICRA), 2014 IEEE International Conference on*, pages 4475–4480. IEEE, 2014.

[9] Kazuya Yoshida. Ets-vii flight experiments for space robot dynamics and control. In *Experimental Robotics VII*, pages 209–218. Springer, 2001.

[10] Jana L Schwartz, Mason A Peck, and Christopher D Hall. Historical review of air-bearing spacecraft simulators. *Journal of Guidance, Control, and Dynamics*, 26(4):513–522, 2003.

[11] Osamu Okamoto, Teruomi Nakaya, and Brett Pokines. Concept verification of three dimensional free motion simulator for space robot. 1994.

[12] Sasi Prabhakaran Viswanathan, Amit Sanyal, and Lee Holguin. Dynamics and control of a six degrees of freedom ground simulator for autonomous rendezvous and proximity operation of spacecraft. In *AIAA Guidance, Navigation, and Control Conference*, 2012.

[13] ByungMoon Kim, Efstathios Velenis, Patrick Kriengsiri, and Panagiotis Tsiotras. A spacecraft simulator for research and education. In *Proceedings of the AIAA/AAS astrodynamics specialists conference*, number 01-367, pages 897–914, 2001.

[14] Dongwon Jung and Panagiotis Tsiotras. A 3-dof experimental test-bed for integrated attitude dynamics and control research. In *AIAA Guidance, Navigation and Control Conference*, volume 5331, 2003.

[15] Dae-Min Cho, Dongwon Jung, and Panagiotis Tsiotras. A 5-dof experimental platform for autonomous spacecraft rendezvous and docking. *AIAA Paper*, 1869, 2009.

[16] D Gallardo and R Bevilacqua. Six degrees of freedom experimental platform for testing autonomous satellites operations. In *Proceedings of the 8th International ESA GNC Conference*, 2011.

[17] Tomasz Rybus, T Barciński, J Lisowski, J Nicolau-Kukliński, K Seweryn, M Ciesielska, K Grassmann, J Grygorczuk, M Karczewski, M Kowalski, et al. New planar air-bearing microgravity simulator for verification of space robotics numerical simulations and control algorithms. In *12th ESA Symposium on Advanced Space Technologies in Robotics and Automation, Noordwijk, The Netherlands*, 2013.

[18] Yoji Umetani and Kazuya Yoshida. Resolved motion rate control of space manipulators with generalized jacobian matrix. *Robotics and Automation, IEEE Transactions on*, 5(3):303–314, 1989.